Journal of Chemical Neuroanatomy, Vol. 4: 373–385 (1991)

Microcomputer-based Three-dimensional Reconstruction of *in situ* Hybridization Autoradiographs

Thomas S. Ford-Holevinski*, Michael R. Castle, James P. Herman and Stanley J. Watson

University of Michigan, Mental Health Research Institute, Ann Arbor, Michigan 48109-0720, USA

ABSTRACT

A number of software routines were written for the public domain Macintosh-based video-densitometry program, Image, to facilitate *in situ* hybridization analysis. These routines utilize fiducial marks drilled in unused portions of the brain to rotate high-magnification images of individual sections so that they may be placed in register. The regions of interest within the registered sections are outlined and intermediate sections interpolated to produce a data set representing a three-dimensional volume. This shell is then filled with the original density data obtained with one or more *in situ* hybridization probes. The final object can be viewed in various degrees of translucency and examined from different angles or computationally resectioned to yield new information concerning activity changes within the region and relationships between reactive sites. These static images can be collected and rapidly displayed as a movie. These routines have been used in this paper to display the differential hybridization of three different mRNA probes in the hypothalamic paraventricular nucleus.

KEY WORDS: Imaging Computerized Analysis Paraventricular nucleus mRNA

INTRODUCTION

In recent years it has become increasingly apparent that the brain is comprised of a chemically heterogeneous collection of interactive nuclei. The association of tasks with individual nuclei occurs rarely, if at all; rather, functions appear to be the province of discrete subsets of neurochemically specified neurons interspersed within and across nuclei. One way of gaining insight into structure–function relationships in the central nervous system is to ascertain which cells in a targeted region actively produce and/or regulate given neurotransmitters/modulators, receptors, or other neuroactive factors implicated in a functional endpoint of choice. *In situ* hybridization (ISH) histochemistry has emerged as an important tool for this analysis of specific neuroactive molecules at discrete sites in the brain. This technique allows visualization of mRNAs encoding a protein of interest at the single-cell level. Further, by virtue of the stoichiometry of DNA–RNA and RNA–RNA hybridization and autoradiographic detection methods, ISH has been used successfully as a quantitative tool to assess changes in mRNA content in response to experimental manipulations.

While capable of demonstrating both localization and regulation of neuronal mRNAs in an anatomical context, to date ISH studies have yielded primarily two-dimensional (2D) results, consisting of series of greyscaled or pseudocolored images illustrating patterns of activity within an individual tissue section (see Schäfer *et al.*, 1991). As the brain is a three-dimensional (3D) organ whose nuclei exhibit pronounced (and sometimes profound) changes across anatomical levels, it is often difficult to determine by these methods subtleties of localization or regulation as one passes through the nuclei of interest. In addition, subnuclear microorganization within chemically identified cell populations is probably specified by connectional properties, which can be difficult to appreciate when viewing individual sections. These relationships can become substantially clearer, however, if the 2D sections, with their binding densities and anatomical reference points, are digitally reassembled and visualized in three dimensions. The surface or overall shape of a nucleus of interest can be examined and, if desired, the volume sliced at alternative angles more appropriate for visualization of selected features. Loci of high activity or density contained within such a structure can be viewed through the surface to gain an appreciation of the relationship between activity and position within the nucleus. Indeed, via such reconstructions, brain regions can be viewed from any angle and set slowly spinning on a screen, allowing insight into novel associations or experimentally induced alterations impossible to detect in a series of sections.

The concept of presenting neuroanatomical data in three dimensions via computerized imaging procedures is hardly new. Though used primarily

*To whom correspondence should be addressed: (313) 764-2113. FAX (313) 747-4130.

0891–0618/91/050373–13 $06.50

by anatomists modeling systems and depicting relationships between individual structures (Prothero and Prothero, 1986), 3D visualization has also been applied to the display of metabolic activity levels (Hibbard *et al.*, 1987) and receptor densities (Santori *et al.*, 1990) within the brain. Over the years, scientists have employed several information input techniques, ranging from the time-consuming tracing of structural edges in photographic plates via digitizing tablets (McLean and Prothero, 1987; Young *et al.*, 1987) to the direct video-digitization of microscopic images and autoradiographic films. After digitization, the next step in reconstructing 3D objects from 2D images is to see that these 2D images are properly oriented with respect to one another (placed in register). This can be done manually during or after image acquisition by rendering one image temporarily translucent and rotating and translating it until it is visually aligned with an adjacent or reference image. Computer-aided alignment has also been performed, occasionally placing fiducial marks in or near the object prior to sectioning (Toga and Arnicar, 1985; McLean and Prothero, 1987). Hoping to nearly eliminate subjectivity, Hibbard and Hawkins (1984) wrote minicomputer software which would align whole rat brain sections using their principal axes. When damaged sections were encountered, they would use a cross-correlation algorithm on the sections to determine the orientation which would give the greatest overlap of features. This technique was well suited to their study of changes in whole brain metabolism. In the case of ISH analysis, however, researchers often focus their attention on anatomically subtle alterations which occur within a given brain structure or region of interest. The images examined are acquired at high magnification and usually contain no brain edges and little in the way of computationally recognizable landmarks.

This having been the case in our study, we chose to drill fiducial holes into the brain, external to the region of interest. Software was written for the Apple Macintosh II series of microcomputer which uses these fiducials to facilitate image registration and animates the sections to display a spinning three-dimensionally reconstructed volume. This pseudo-solid can be rendered on the screen using nearest-point (surface), brightest-point, or mean-value projection models and enhanced with depth (distance) cues or partial surface opacity. Similar projection and enhancement techniques have previously been implemented on other hardware platforms (Robb, 1988).

To demonstrate the utility of the 3D reconstruction software, we have chosen to examine in detail the expression of neuropeptide mRNAs in the hypothalamic paraventricular nucleus (PVN), a well-characterized region of the brain which exhibits considerable local microheterogeneity. In our analysis, we present data from an animal which has received bilateral adrenalectomy. This experimental paradigm has well-known consequences on the expression of neuropeptide mRNAs in distinct subregions of this nucleus, including an increase in corticotropin-releasing hormone (CRH) mRNA levels and an induction of arginine vasopressin (AVP) mRNA in the medial parvocellular zone of the PVN, with no changes in oxytocin (OXT) or AVP mRNA content in the immediately adjacent posterior magnocellular PVN (Wolfson *et al.*, 1985; Young *et al.*, 1986; Schäfer *et al.*, 1989). Utilizing these probes in an adrenalectomized animal, we can therefore visualize mRNA species restricted primarily to the medial parvocellular region of the PVN (CRH) and the posterior magnocellular (OXT) PVN or distributed across both regions (AVP). This level of analysis allows the visualization and reconstruction of species obeying, for the most part, defined anatomical subdivisions of this heterogeneous brain region.

MATERIALS AND METHODS

Animal handling

Male Sprague–Dawley rats, weighing between 250–300 g, were utilized in this study. Animals were adrenalectomized via a dorsal approach. All animals were maintained on 0.9% saline in an animal quarter with controlled temperature and humidity. Rats were killed by decapitation 4 days following adrenalectomy, the brains removed and rapidly frozen in isopentane ($-40°C$). The brains were kept at $-70°C$ until prepared for sectioning.

Fiducial apparatus

Fiducial holes were drilled in the frozen brains using the apparatus shown in Fig. 1. This Plexiglas device consists of a small open box into which the chuck and frozen brain are clamped and an adjustable upper plate with a portion of a 21-gauge hypodermic syringe needle embedded in it to act as a drill guide. The brains were secured to the chuck with OCT mountant and the chuck was secured in the chilled fiducial apparatus. The apparatus and brain remained in the cryostat while holes were drilled with a #80 drill bit (0.0135-in) held in a Dremel tool slowed by a variable transformer. The upper plate of the fiducial apparatus was secured by wing nuts and washers on studs drilled into platforms glued on the sides of the lower box. The attachment holes in the upper plate were 2 cm in diameter to allow the drill guide to be positioned over any portion of the frozen brain. Fiducial holes were drilled in both upper quadrants and one lower quadrant of the brain, as far from the area under investigation as possible. A final brain section with fiducial holes is shown in Fig. 2.

In situ hybridization

Frozen rat brains with fiducial marks were sectioned on a Slee cryostat. Consecutive frozen 15-μm thick

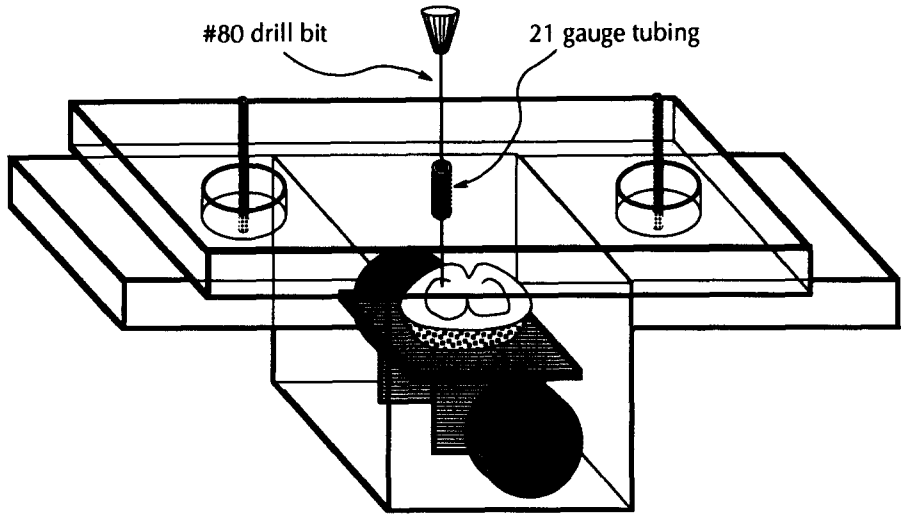

Fig. 1. Apparatus used to bore fiducials in frozen rat brains.

Fig. 2. Low-power image of a Nissl-stained section from a brain which was prepared with fiducial holes (arrows) using the apparatus in Fig. 1.

sections were taken through the region of the hypothalamus. All sections were thaw-mounted onto poly-L-lysine (Sigma)-coated slides and stored at −70°C until processing. Consecutive sections were taken at 50-μm intervals and processed for ISH using probes directed against AVP, OXT and CRH mRNAs.

In situ hybridization was performed on sections sampled through the region of the PVN. Sections were removed from the −70°C freezer, fixed for 30 min in 4% paraformaldehyde, rinsed three times in 2X SSC and deproteinated with 0.1 μg/ml proteinase K for 15 min at 37°C. After deproteination, slides were washed for 1 min in distilled H_2O, 1 min in 0.1 M-triethanolamine, and 10 min in 0.1 M-triethanolamine containing 0.25% acetic anhydride. The latter acetylation steps reduce electrostatic binding of cRNA probe to tissue sections. Deproteinated, acetylated sections were rinsed in distilled H_2O and dehydrated through graded alcohols.

Antisense ^{35}S-labeled cRNA probes for proAVP exon C (courtesy of T. Sherman, University of Pittsburgh), proOXT exon C (courtesy of T.

Sherman) and proCRH exon 2 (courtesy of R. Thompson, University of Michigan) were produced using the SP6 transcription system. Plasmids containing subcloned cDNA fragments were linearized with the appropriate restriction enzyme to yield probes of desired length and G:C composition. The labeling reaction mixture contained 1 μg linearized plasmid, 1X-SP6 transcription buffer (Bethesda Research Labs), 250 μCi [α-^{35}S]UTP (> 1000 Ci/mmol, dried; Amersham), 150 μM-ATP, 150 μM-CTP, 150 μM-GTP, 12.5 mM-dithiothreitol (DTT), 3.0 units/μl RNAsin (Promega) and 0.5 units/μl SP6 RNA polymerase (Promega). The reaction was incubated for 90 min at 37°C, and the labeled probe separated from free nucleotide over a Sephadex G50-50 column equilibrated in 0.1 M-Tris–HCl, pH 7.5, 12.5 mM-EDTA, 0.15 M-NaCl, 0.2% SDS and 10 mM-DTT. The AVP probe was a 225 bp cRNA coding for the C-terminal region of the proAVP molecule. The OXT probe was a 169 bp cRNA coding for the C-terminal region of the proOXT molecule. Sequences chosen for construction of AVP and OXT probes showed no significant homology. The CRH cRNA was a 770 bp probe derived from exon 2 of the rat CRH gene.

^{35}S-labeled cRNAs were diluted in hybridization buffer (75% formamide, 10% dextran sulfate, 3X SSC, 50 mM sodium phosphate buffer, pH 7.4 1X Denhardt's, 0.1 mg/ml yeast tRNA and 0.1 mg/ml sheared salmon sperm DNA) to yield 1 000 000 dpm/30 μl. Aliquots of 30 μl were applied to each section, the sections were coverslipped and the coverslips sealed with rubber cement. Slides were incubated at 55°C in sealed plastic boxes containing moistened foam. Following an overnight hybridization, the coverslips were removed, the slides rinsed in 2X SSC and immersed in fresh 2X SSC for 20 min. The tissue was treated with RNase A (200 μg/ml) at 37°C for 30 min to degrade any remaining single-stranded cRNA. Sections were then washed successively in 2X, 1X and 0.2X SSC for 10 min each, followed by a 60 min wash in 0.2X SSC at 65°C. Sections were dehydrated through alcohols, exposed to Kodak XAR X-ray film, and emulsion-dipped in Kodak NTB2 nuclear emulsion. Emulsion-dipped sections and standards were exposed for 7 days (AVP, OXT) or 21 days (CRH); batch development was based on the signal strength and signal-to-noise ratio of test slides developed at regular intervals.

Image acquisition and analysis hardware

The videomicroscopic images were acquired with an Apple Macintosh II microcomputer and a Data Translation DT2255 QuickCapture video frame grabber attached to a Dage–MTI Series 68 video camera. A Wild Makroskop M420 was used to capture the low-power (8X) images while a Leitz Orthoplan microscope equipped with a Minnesota Datametrics Microscope Digitizer (to record relative stage coordinates) was used for the higher magnifications (79X). Subsequent analysis and reconstruction was performed on either an Apple Macintosh II, IIci or IIfx microcomputer, each of which contained 8 megabytes of RAM.

Image analysis software

The software used for the majority of this analysis was the Macintosh-based public domain program, Image, written by Wayne Rasband at the National Institutes of Health (NIH). With it one can acquire, save and print video images; draw regions of interest and obtain densitometric readings which may be automatically converted to final values using a calibration curve; enhance the images using several image processing filters; annotate the images; animate collections of images as movies; and perform other functions, too numerous to describe here. The program contains a built-in macro language permitting complicated, repetitive procedures to be converted to single commands. The included source code allows customization or the addition of entirely new features, as we demonstrate here.

Image capture

Before capturing the image, the slide containing a mounted brain section was placed on the microscope stage, the fiducial hole in the upper left quadrant was centered in view using brightfield lighting at 79X, and the microscope digitizer (stage coordinate apparatus) was zeroed. The other fiducial holes were then centered in view and the stage coordinates of each recorded in a Microsoft Excel spreadsheet on the Macintosh. The spreadsheet both stored the values and determined the distances between each pair of fiducial holes, alerting us of possible deformations in the section. Annotations were also included in the sheet to indicate, for example, whether a fiducial hole should not be used due to tissue damage between the hole and the region of interest.

The area of the brain containing the PVN was then centered, the microscope illumination switched to darkfield to display the exposed silver grains in the emulsion layer, and the view of the hybridization data centered and focused on the computer screen. A 16-frame average image was captured and saved (Fig. 4A) and the coordinates of this image recorded in the spreadsheet. This procedure was repeated for all sections containing reactivity in the PVN region. In addition to the PVN images, a background darkfield image (identical setup minus the microscope slide) was acquired for each imaging session. This image was subtracted from each of the images acquired during that session. Low-power brightfield images were also acquired using the Wild Makroskop with the same camera and microcomputer (Fig. 2). Locations of the fiducial holes, all visible in these low-magnficiation images, were

recorded using screen coordinates from the digital images rather than microscope stage coordinates.

RESULTS

Image registration

In order to reconstruct a 3D volume of a region of the sectioned brain, the captured images must be rotated and translated so that they all share a common coordinate system (Toga, 1990). This image registration was accomplished by aligning the fiducial marks from each image in the set with those from a reference image (in this case the most vertically oriented section) selected from the group. To find the rotation required for registration, a simple trigonometric calculation was performed to find the angle formed by the line segment connecting a pair of fiducial points in the current image and the segment connecting the corresponding two fiducials in the reference image (Fig. 3A). To minimize rotation errors which could be caused by unnoticed folds, tears, regions of compression, or other deformations, the angles formed by all of the available corresponding pairs of visibly unaffected fiducial holes were averaged to find the required angle of rotation. This procedure allowed rotation to occur even in those cases where a fiducial hole had been damaged, drilled through a ventricle, or listed as questionable for other reasons. Once the angle had been determined, existing Image code was used to rotate the current image into register with the reference image. The mathematics of image rotation, translation, and other transformations have been described extensively in the literature (Foley and Van Dam, 1984).

Code was also written to use the fiducial hole coordinates and the coordinates of the PVN images to translate the images (i.e., move them horizontally and vertically without rotation) to the proper location relative to a reference image. This routine was used very successfully on the traced edges of the low-power brightfield images (Fig. 3B) and was accurate to one or two pixels when applied to a single test image that was translated and rotated to several different angles. Frozen sections, however, are subject to physical deformations and are easily damaged. When serial sections of rat brain were used, the registered images were judged to have been properly rotated, but their translations deviated from the desired placement by as many as 40 pixels in the x and y directions at 79X magnification. For this reason, the rotated images were manually translated, using the third ventricle as a feature common to all sections.

The compression artifact was a common deformation and was observed in variations of the calculated inter-fiducial distances whose values should be constant. Whereas the range of values obtained for the two fiducials parallel to the cutting edge varied by only 3.3% (8.513 mm to 8.796 mm or about 113 pixels at 79X), those fiducials perpendicular to the knife varied by nearly 14.5% (3.170 mm to 3.652 mm or about 193 pixels). While differences of this magnitude might cause rotational errors of only one or two degrees, they could easily be responsible for the unacceptably large translational errors.

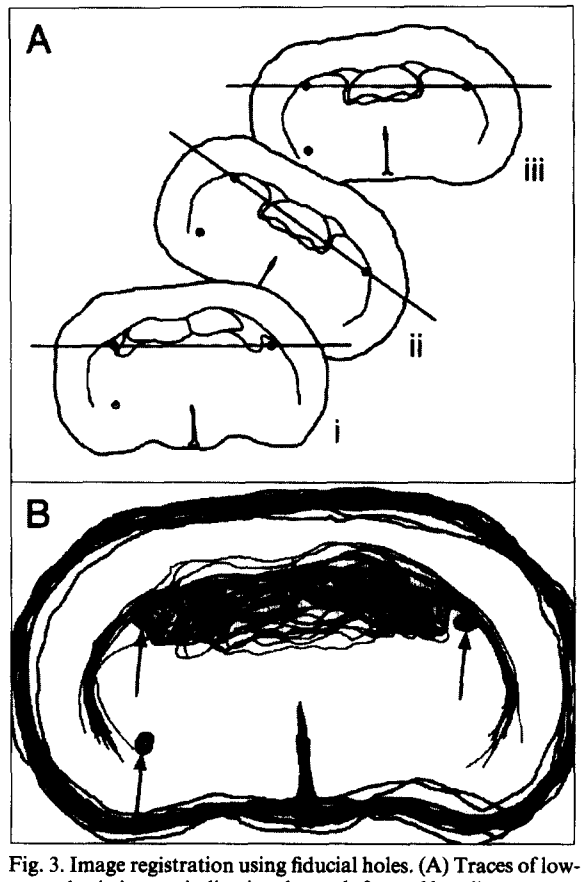

Fig. 3. Image registration using fiducial holes. (A) Traces of low-power brain images indicating the angle formed by a line segment connecting the upper fiducial holes. (i) Reference image, (ii) unrotated section, (iii) section after rotation. (B) The summation of all low-power whole brain traces after each was rotated and translated by the software to be in register with a reference trace.

Construction of the data sections to be used in the 3D reconstruction

After all of the sections were digitized (CRH, OXT and AVP probe-hybridized and Nissl-stained), image files were opened in Image and regions of interest (ROIs) were drawn around the areas showing activity or the proper cellular patterns. These ROIs were saved for later use. When we found that there were no cases in which the ROIs for one probe would include all of the data from the other image sets, we decided to combine them. There were 51 sections which were judged to contain a positively labeled portion of the PVN. These could be divided into 11 sets of images, set at approximately 50 μm intervals, each of which contained a Nissl-stained section and up to three adjacent sections containing activity corresponding to the hybridization of

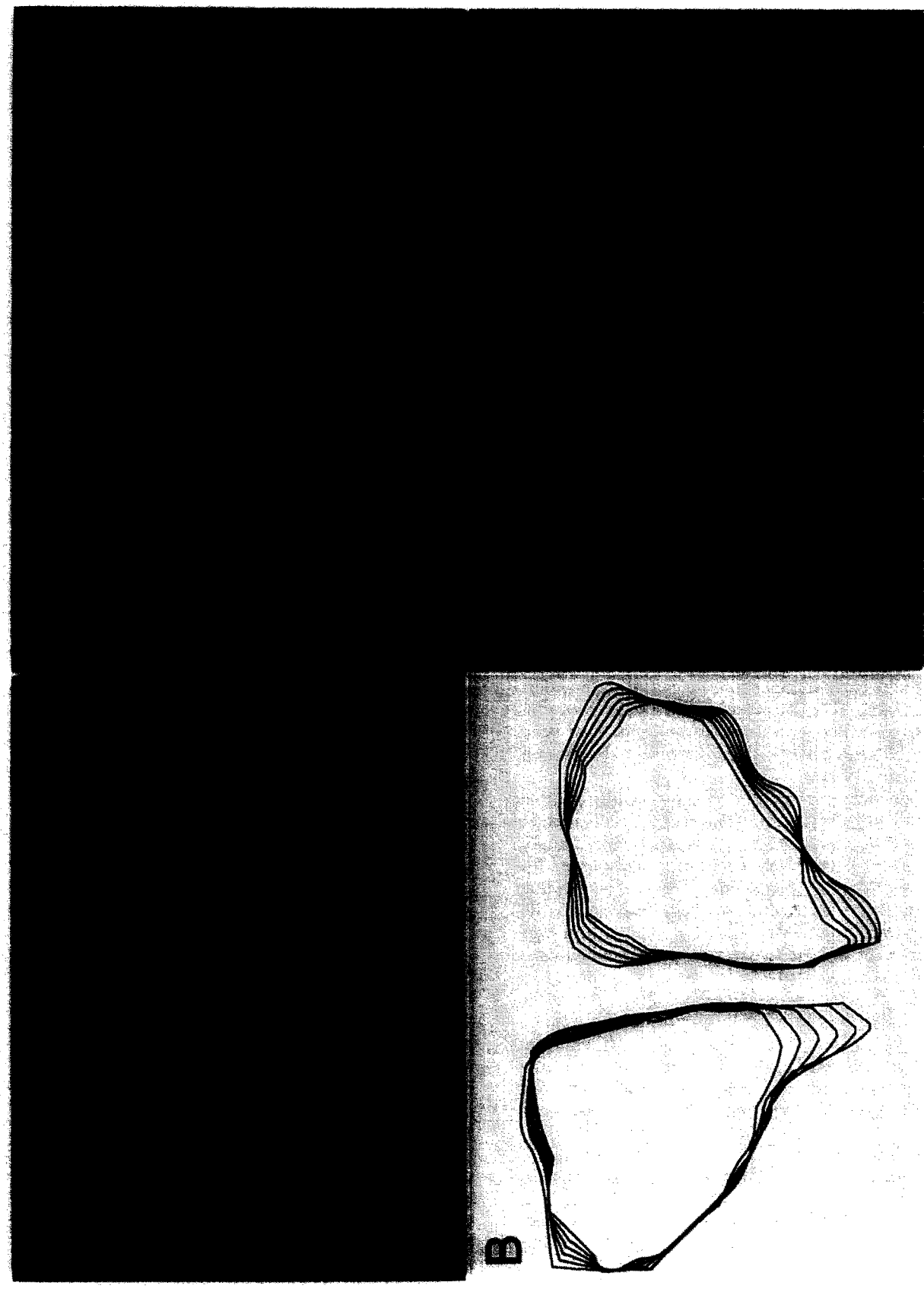

Fig. 4. Preparation of the final images used in the 3D reconstruction. (A) Darkfield image of the area encompassing the PVN at a microscopic magnification, 79X. (B) Intermediate section ROI outlines formed using the blend tool in Adobe Illustrator. (C) Interpolated ROI outline from (B) filled with a grey value of 10 and outlined with a grey value of 20 to form surface of PVN in final reconstruction. (D) ROI outline replaced with actual data from darkfield image (A).

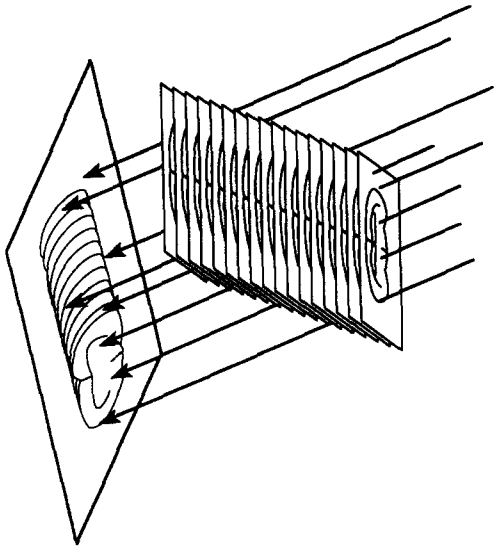

Fig. 5. Ray projection. Parallel rays pass through the data set at an angle determined by the user to display the values encountered on an imaging plane in a manner dependent on the chosen projection method.

probes for CRH, AVP and OXT mRNA. We used the union of ROIs for each of the 11 sets to define the outermost limits of the PVN in those 11 planes.

In order to create a 3D pseudo-object with smooth contours, it was necessary to generate the ROIs in the sections that would lie between the 11 planes. Image currently lacks the capacity to interpolate the required outlines. For this task, the 11 summed outlines were converted from bit maps to defined curves or objects using the Streamline program from Adobe. The required intermediate ROI curves were then automatically generated using the blend tool in the Adobe Illustrator program (Fig. 4B). Once these ROIs had been generated we decided to fill them with a constant dark grey value with a slightly lighter border (Fig. 4C) so that they would produce an obvious edge during rotation without obscuring the actual data points contained in the pseudo-solid. Although Image contains the functionality necessary to perform this task, its inability to read the files produced by Adobe Illustrator led us to use PhotoShop, an image processing program, also from Adobe, to generate the complete set of grey-filled ROIs and then fill the ROIs from the appropriate sections with the original darkfield data (Fig. 4D).

Planar projection of the reconstructed volume: software features

Once the images were in proper register, we began to produce the projection sequence. Each frame of the animation sequence was a projection of the 3D data set onto a plane from a different viewing angle. To visualize this, imagine a field of parallel rays passing through a volume enclosing one or more solid objects and striking a screen oriented normal to the direction of the rays. Each ray projects a value onto the screen, or projection plane, based on the values of points from the volume in its path (Fig. 5). We had three methods at our disposal for calculating the projections onto this plane: nearest-point, brightest-point and mean-value projection. The choice of projection technique and the settings of various visualization parameters in our software together determine how both surface and interior structures will appear.

Nearest-point projection

The nearest-point projection method uses a z-buffer hidden surface elimination algorithm (Foley and Van Dam, 1984) to produce an image of the surfaces visible in the volume from the current viewing angle. At each point in the projection plane, a ray passes normal to the plane through the volume. The value of the nearest non-transparent point which the ray encounters in the volume is stored in the projection image. The collection of these nearest points defines the surface of the object under examination (Fig. 6A and D).

Brightest-point projection

The brightest-point projection method examines points along the same rays, projecting the brightest point along each ray onto the projection image. This algorithm will display those objects with the greatest optical density (such as bone in a computed tomographic study, Fig. 6C; or ISH data, Fig. 6E).

Mean-value projection

A modification of this projection method, mean-value projection, sums the values of all non-transparent points along each ray and projects their mean value. Although the latter tends to return images with softer edges and lower contrast, it could be useful when attempting to visualize objects contained within a structure of higher density (e.g. a skull).

The ability to combine these projection methods, to work with subsets of the original data, to make some uninteresting structures transparent, and to provide depth cues for the visible portion of the data facilitates the study of volumes of interest and offers the viewer the potential for a high degree of visual realism.

Opacity

Sometimes, the location of a structure with respect to other structures in a volume using brightest-point or mean-value projection is not clear. The opacity visualization parameter permits the display of weighted combinations of the nearest-point projection with either of these other two methods, often giving the observer the ability to view inner structures through translucent outer surfaces of the reconstructed volume.

Rotation of projections

Rotational visualization parameter settings control the initial rotation angle, the angle increment between rotations, and the total angle of rotation of the reconstructed volume. Our program projects the volume onto the viewing plane at each incremental rotation, beginning with the volume rotated by the initial angle about the axis of rotation and ending once the volume has been rotated further by the total angle. The smaller the angle increment, the smoother the animation (at the cost of consuming more memory). Setting the total angle at 360 degrees produces a movie which displays the volume from all sides (Fig. 7). Animation of a series of images produced at several consecutive angles immediately reveals relationships between objects in the volume (such as left–right differences and front–back asymmetry) which are often difficult to observe in individual projections. Using a Macintosh IIfx, a projection of 90 views at 4-degree increments of a data set containing 52 images of size 350 by 240 pixels took 90 min. If the rate of technological advancement observed over the last decade continues, this time will be cut at least in half on future machines in each of the next few years.

Transparency thresholds

Upper and lower transparency threshold parameters determine the transparency of structures in the volume. Projection calculations disregard points having values less than the lower threshold or geater than the upper threshold. Setting these thresholds permits making background points (points not belonging to any structure) invisible. By setting appropriate thresholds, one can strip away layers having reasonably uniform and unique intensity values and highlight (or make invisible) inner structures. With computed tomographic data, skin could be removed to reveal the surface of the skull (Fig. 6B). With ISH data, areas of low activity could be removed to reveal the centers of greatest hybridization and their proximity to one another.

Depth cues

Depth cues can further contribute to the 3D quality of projection images by giving perspective to projected structures (Fig. 6A–D and F). The depth-cueing visualization parameters determine whether projected points (in nearest-point and brightest-point projections) originating near the viewer appear brightest, while points farther away are dimmed linearly with distance from the nearest points in the volume. The trade-off for this increase in realism is that the data points shown in a depth-cued image no longer possess accurate densitometric values. In the static frames of Fig. 7, depth cues enhance the appearance of pseudo-object rotation.

Illustrative example: 3D reconstruction of the PVN

The data-filled PVN volumes projected in this study (Fig. 8) clearly recapitulate the known distributions of AVP, OXT and CRH mRNAs in the adrenalectomized rat. One can visualize the rather subtle differences among these peptide mRNAs in terms of localization to magnocellular vs parvocellular regions of the PVN. For example, as previously documented (cf. Swanson and Sawchenko, 1983), AVP and OXT are differentially distributed across the posterior magnocellular PVN. AVP has a predominantly posterior and lateral orientation, while OXT is preferentially localized anteromedially, having particularly dense aggregations of cells in the ventral-most aspect of this PVN subdivision. Interestingly, OXT exhibits a striking density of large cells localized in the dorsal 'cap', which continue through the nucleus to the posterior extent of the PVN. These correspond to 'magnocellular' neurons projecting to brainstem and spinal cord sites involved in autonomic regulation. In contrast, the presence of AVP in this region is more circumspect and clearly does not extend as far posteriorly as the OXT cells. This pronounced difference between OXT and AVP in this region implies a far more powerful input of OXT on brainstem and spinal cord neurons involved in central autonomic regulation.

Rich localization of CRH-positive cells is clearly evident in the dorsal aspect of the medial parvocellular PVN, corresponding to the known localization of cells projecting to the median eminence. As one proceeds through the nucleus, the cell group begins as a loose aggregation of cells anteriorly and gradually coalesces into a tight bundle of neurons oriented at an obtuse angle to the wall of the third ventricle. AVP mRNA can also be seen in the medial parvocellular PVN of an adrenalectomized rat, as has been shown previously (Wolfson *et al.*, 1985; Schäfer *et al.*, 1989). Yet, it is evident that only a subset of neurons containing CRH are in a position to coexpress AVP mRNA, and indeed, that these cells are predominantly located dorsomedially. This

Fig. 6. Projection styles. (A) Computed tomographic (CT) series projected at an angle of 24° from the top using nearest-point projection, depth cueing, and no density thresholding. (B) CT series projected as in (A), adding density thresholding to eliminate surface tissues. (C) CT series projected at an angle of 60° from the top using the brightest-point method and depth cueing. (D) A single lobe of the PVN incorporating OXT hybridization data projected at 204° from the front using the nearest-point method and depth cueing. The observed surface is due primarily to the grey-filled ROI images in the data set. (E) The data set and angle in (D) projected using the brightest-point method without depth cueing. The data values are accurately displayed, but their orientation to the viewer is not obvious in this static image. (F) The same conditions as (E) with the addition of depth cueing. The data values are no longer accurate, but it is now easy to see which points are closest to the viewer.

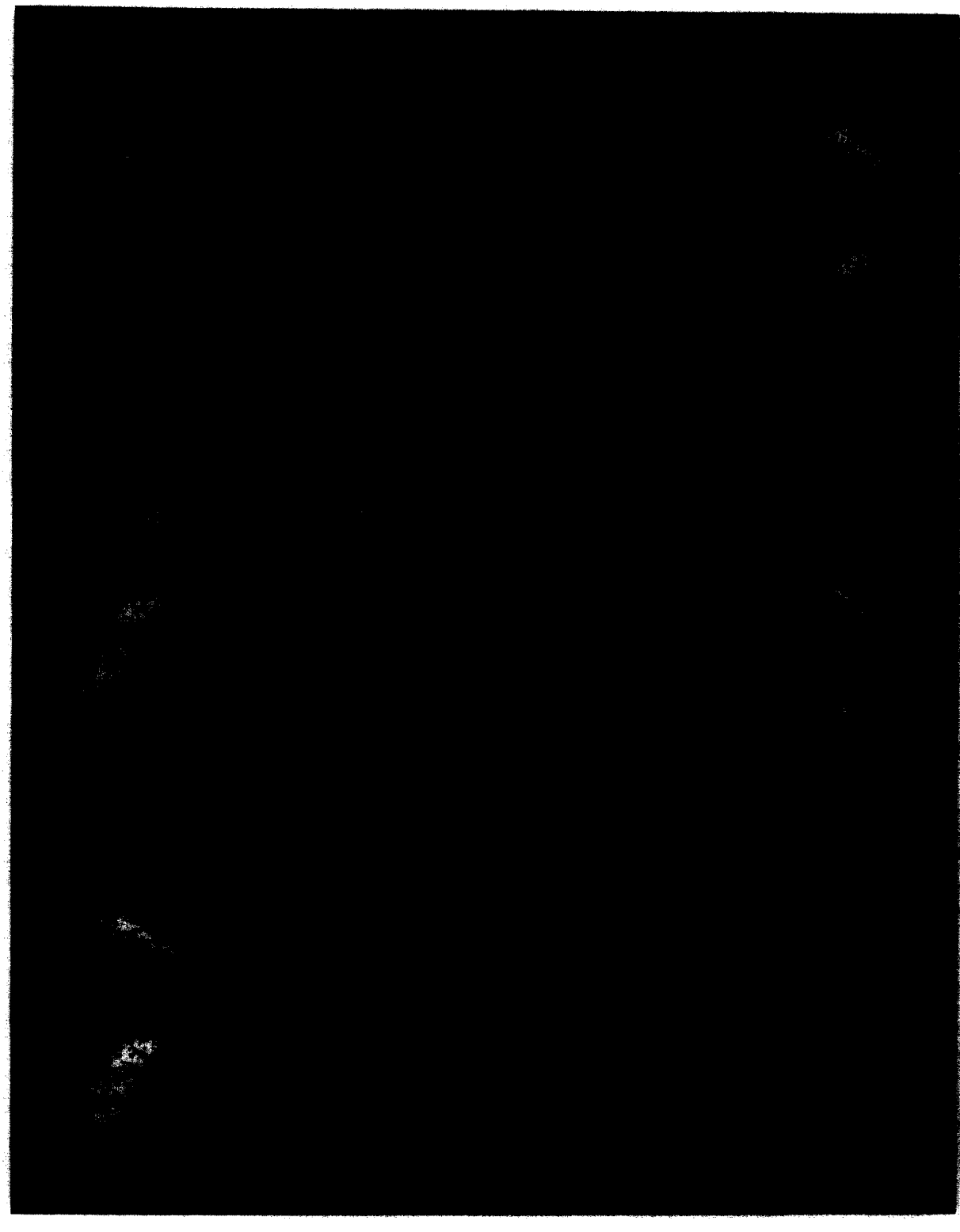

Fig. 7. Several frames of a movie showing OXT hybridization data in both lobes of the reconstructed PVN. The projection technique is the same as Fig. 6F.

Fig. 8. Three-dimensional representations showing that the sites of hybridization vary widely with the probe employed. (A) A single lobe of the PVN incorporating OXT hybridization data and projected at 204° from the front using the brightest-point method and depth cueing. (B) The same projection as (A) with the exception that the data incorporated are from CRH hybridization. (C) The same projection as (A) with the exception that the data incorporated are from AVP hybridization.

differential localization points toward specialization of neurons within the already circumscribed population of neurons in the medial parvocellular PVN, with some CRH cells capable of expressing AVP in response to glucocorticoid removal and others refractory to this treatment. The parcellation of these classes of cells to specific subregions of the medial parvocellular PVN implies an important anatomical differentiation of these cell types, perhaps due to differences in neuronal connectivity.

DISCUSSION

Data display

We have demonstrated that it is possible to use a microcomputer to reconstruct in 3D a region of ISH activity from 2D brain sections. We now possess the means for generating movies of these spinning pseudo-objects relatively quickly and inexpensively. It is fortunate for us that ISH data are comparatively pointile in nature, for this allows us to display simultaneously nearly all of our data with both positional and densitometric accuracy. This is in contrast to metabolic rate studies in which the data in each slice obscure the data in the slice behind it. In those cases investigators have been forced to project the activity onto the surface of the object, display only the data in excised regions (Toga and Arnicar-Sulze, 1987) or reduce their data set to a series of isocontour lines and display the data as a wire frame image (White *et al.*, 1990). None of these visualization techniques lends itself as well to cinematic display.

In this presentation we elected to draw ROIs, going to great lengths to include only the data within and generate constant grey ROIs for intermediate sections. Although this made it possible to observe the data within a PVN with well-defined edges, one could instead choose to exert minimal effort and reconstruct a volume using only the rotated and translated darkfield images. Rather than a spinning solid object, the viewer would observe a volume more closely resembling a spinning field of stars. To all but the purist, this approach would probably be less visually appealing. However, it would take only a fraction of the time and might be a reasonable technique for screening data before entering the next, time-consuming steps.

Although more studies of this type are moving to workstations and personal computers (Smith, 1987; Young *et al.*, 1987; Geist and Vannier, 1989), the computational intensity of this reconstruction task has forced the vast majority to perform their studies on much more expensive systems (Hibbard and Hawkins, 1984; Toga and Arnicar-Sulze, 1987; White *et al.*, 1990). Our software runs on the Apple Macintosh II series of personal microcomputer. While faster microcomputers may be available, this machine has certain advantages. It has a very strong graphics orientation and is widely regarded as being a sophisticated yet easy-to-use computing tool. Its ability to run several programs at a time, for example, allows the user to effortlessly switch between image capture and manipulation, spreadsheet and statistical analyses, graphics and other drawing tasks, and word processing. Finally, the powerful NIH Image program, its source code, and the routines that we and others have added to it, are all available at no cost.

Fiducials and image registration

There are several good reasons to put fiducial holes in the sections, provided that they can be added without endangering any ROIs. When viewing regions without good structural landmarks at higher magnifications, it can be nearly impossible to accurately place adjacent sections in register. Even if

the nature of the tissue preparation makes automatic translation difficult, automatic image rotation is usually worth the slight additional effort and may even improve the chances of successful manual image translation. Unlike natural tissue landmarks, the fiducial holes are found in every section and are, within some experimental error, in the same location in each. Eventually we hope our software will use the relationships between these holes to correct simple compression distortions in the sections, rendering automatic translation of high-magnification images more plausible.

What comes next?

Our immediate plans include supporting the simultaneous display of data obtained from multiple probes, giving each a different primary color. When these are combined and projected, the result will be a color movie of the pseudo-solid, displaying the relationships between the sites of reactivity. On-the-fly image compression and improved memory management capabilities are now being added to the system software of the Macintosh which will enable the production of more realistic animations of much greater length.

Eventually we hope to be able to click on any point in a 3D view and have the coordinates and density value returned, thereby using the 3D view as a map to extract information from the complete data set. We also plan to add the ability to interpolate intermediate sections in Image, removing the need for both Illustrator and PhotoShop in our analysis. It should then be possible to automate a great deal of this work using the macro language available in Image.

After that, the next major step will involve the averaging of data sets from several animals. Once averaged image sets are obtained, it will be possible to compare control and experimental groups using statistical techniques. We could reconstruct pseudo-solids which would display the variance between the sets showing at-a-glance where a treatment has produced a change in activity. This will probably require the warping of the image sets to a standard so that they might be averaged and compared (Bookstein, 1990).

CONCLUSION

The model used for the development of our reconstruction scheme elegantly illustrates the utility of this method for gaining an appreciation of anatomical interrelationships among neuroactive substances at a subnuclear level. Our data clearly recapitulate previous reports in the literature derived from careful inspection and mapping of 2D microscope images and resolves subtle differences known to exist among localization of neuropeptide mRNAs within these defined regions of the PVN. Application of this method to uncharacterized neuroactive substances or to regions where the distribution of such substances is ill-defined will allow for rapid assignment of these principals to specified anatomical locations. With the addition of densitometric data, one can further resolve the relative abundance of these substances within an individual nucleus, and also begin to address, between animals, issues of intra-nucleus regulation of mRNAs for neurotransmitter/modulators, receptors and growth factors in response to physiological or pharmacological manipulations. Similarly, these reconstruction methods may be extremely helpful in combination with lesion and/or tract tracing techniques to assess localization and regulation of neuroactive principals across definable neuroanatomical circuits.

ACKNOWLEDGEMENTS

This work was supported by MH42251, DA02265 and the Lucille P. Markey Charitable Trust. The authors would like to thank Wayne Rasband (the author of Image), Richard Griggs for the construction of the fiducial apparatus, and Janice Keller, Seung Kwak, James Stewart, Don Beery and Sharon Burke for technical assistance.

REFERENCES

Bookstein, F. L. (1990). Distortion correction. In *Three-Dimensional Neuroimaging* (ed. Toga, A. W.), pp. 235–249. Raven Press, New York.

Foley, J. D. and Van Dam, A. (1984). *Fundamentals of Interactive Computer Graphics*, Addison-Wesley, Reading, Massachusetts.

Geist, D. and Vannier, M. W. (1989). PC-based 3-D reconstruction of medical images. *Comput. & Graphics* **13,** 135–143.

Hibbard, L. S. and Hawkins, R. A. (1984). Three-dimensional reconstruction of metabolic data from quantitative autoradiography of rat brain. *Am. J. Physiol.* **247,** E412–E419.

Hibbard, L. S. and Hawkins, R. A. (1988). Objective image alignment for three-dimensional reconstruction of digital autoradiograms. *J. Neurosci. Meth.* **26,** 55–74.

Hibbard, L. S., McGlone, J. S., Davis, D. W. and Hawkins, R. A. (1987). Three-dimensional representation and analysis of brain energy metabolism. *Science* **236,** 1641–1646.

Huijsmans, D. P., Lamers, W. H., Los, J. A. and Strackee, J. (1986). Toward computerized morphometric facilities: A review of 58 software packages for computer-aided three-dimensional reconstruction, quantification, and picture generation from parallel serial sections. *Anat. Rec.* **216,** 449–470.

McLean, M. R. and Prothero, J. (1987). Coordinated three-dimensional reconstruction from serial sections at macroscopic and microscopic levels of resolution: The human heart. *Anat. Rec.* **219,** 434–439.

Prothero, J. S. and Prothero, J. W. (1986). Three-dimensional reconstruction from serial sections: IV. The reassembly problem. *Comp. Biomed. Res.* **19,** 361–373.

Robb, R. A. (1988). Multidimensional biomedical image display and analysis in the biotechnology computer resource at the Mayo Clinic. *Machine Vision and Applications* **1,** 75–96.

Santori, E. M., Samaie, M. and Toga, A. W. (1990). Receptor binding: Imaging beyond the third dimension. In *Three-Dimensional Neuroimaging* (ed. Toga, A. W.), pp. 103–121. Raven Press, New York.

Schäfer, M. K.-H., Herman, J. P. and Watson, S. J. (1991). *In situ* hybridization histochemistry. In *Imaging in the Functional Neuroanatomy of Drug Action* (ed. London, E. D.). Telford Press, West Caldwell.

Schäfer, M. K.-H., Herman, J. P. and Watson, S. J. (1989). *In situ* hybridization analysis of gene expression in the HPA axis: Regulation by glucocorticoids. In *Wenner-Glenn International Symposium Series*, pp. 11–22. The Macmillan Press, New York.

Smith, R. G. (1987). Montage: a system for three-dimensional reconstruction by personal computer. *J. Neurosci. Meth.* **21,** 55–69.

Swanson, L. W. and Sawchenko, P. E. (1983). Hypothalamic integration: Organization of the paraventricular and supraoptic nuclei. *Ann. Rev. Neurosci.* **6,** 269–324.

Toga, A. W. (1990). Three-dimensional reconstruction. In *Three-Dimensional Neuroimaging* (ed. Toga, A. W.), pp. 189–210. Raven Press, New York.

Toga, A. W. and Arnicar, T. L. (1985). Image analysis of brain physiology. *Comput. Graph. Appl.* **5,** 20–25.

Toga, A. W. and Arnicar-Sulze, T. L. (1987). Digital image reconstruction for the study of brain structure and function. *J. Neurosci. Meth.* **20,** 7–21.

White, W. F., O'Gorman, S. and Roe, A. W. (1990). Three-dimensional autoradiographic localization of quench-corrected glycine receptor specific activity in the mouse brain using ^{3}H-strychnine as the ligand. *J. Neurosci.* **10,** 795–813.

Wolfson, B., Manning, R. W., Davis, L. G., Arentzen, R. and Baldino, F. Jr. (1985). Co-localization of corticotropin releasing-factor and vasopressin mRNA in neurons after adrenalectomy. *Nature* **315,** 59–61.

Young, S. J., Royer, S. M., Groves, P. M. and Kinnamon, J. C. (1987). Three-dimensional reconstructions from serial micrographs using the IBM PC. *J. Elect. Micro. Tech.* **6,** 207–217.

Young, W. S., Mezey, E. and Siegel, R. E. (1986). Quantitative *in situ* hybridization histochemistry reveals increased levels of corticotropin releasing factor mRNA after adrenalectomy in rats. *Neurosci. Lett.* **70,** 198–203.